Annals of Nuclear Medicine Vol. 8, No. 4, 269–276, 1994

Evaluation of the ventilation-perfusion ratio in lung diseases by simultaneous anterior and posterior image acquisition

Yasunobu NAKATA, Isamu NARABAYASHI, Kozo SUEYOSHI, Ritsuo MATSUI, Ryuichiro NAMBA and Kojiro TABUCHI

Department of Radiology, Osaka Medical College

Ventilation and perfusion images were acquired during tidal breathing using ^{81m}Kr gas and ^{99m}Tc-MAA. Anterior and posterior functional images of $\dot{V}/\dot{Q}$ and $\dot{Q}/\dot{V}$ were simultaneously acquired in 34 subjects with various lung diseases and 6 healthy controls. Superimposed anterior and posterior images were constructed and histograms of the frequency distribution for ventilation, perfusion, and the $\dot{V}/\dot{Q}$ ratio were displayed for both lungs as well as for the left and right lungs individually. Blood gas analysis and general lung function tests were also performed on the day before scintigraphy. A correlation between marked uneven distribution of $\dot{V}/\dot{Q}$ and A-aDO_2 was found. When the proportion of counts at $\dot{V}/\dot{Q} < 0.67$ and/or $\dot{V}/\dot{Q} > 1.50$ in the $\dot{V}/\dot{Q}$ counts histogram was compared with A-aDO_2, there was a significant positive correlation for anterior images ($r = 0.684$, $p < 0.05$), posterior images ($r = 0.654$, $p < 0.05$) and superimposed images ($r = 0.696$, $p < 0.05$). Superimposed images therefore showed the highest correlation. There was no correlation between the results of lung function testing and A-aDO_2. Coronal SPECT images were also obtained in 15 patients and compared with the superimposed anterior and posterior planar images. There was a good correlation ($r = 0.888$, $p < 0.001$) between both the imaging methods regarding the marked uneven distribution of $\dot{V}/\dot{Q}$. Simultaneous anterior and posterior planar image acquisition reduces the examining time, is simple, and is noninvasive. The present results also suggest that it is useful for quantitative evaluation of the ventilation-perfusion ratio.

Key words: Ventilation-perfusion image, V&P SPECT, ^{81m}Kr gas, ^{99m}Tc-MAA, $\dot{V}/\dot{Q}$ mismatch

INTRODUCTION

IN PREVIOUS STUDIES, $\dot{V}/\dot{Q}$ mismatch has chiefly been assessed by means of the posterior image, but in a localized disease such as lung cancer, regional ventilation is as important as regional perfusion for understanding the influence on gas exchange. A better understanding of the pathophysiology of such diseases is useful in determining the indications for an operation and in judging the effect of treatment.[1–3] In the present study, we assessed the ventilation-perfusion ratio with coronal SPECT images or simultaneous anterior and posterior image collection. We then produced histograms of the data and investigated the clinical value of our methods.

Received May 27, 1994, revision accepted August 4, 1994.
For reprint contact: Yasunobu Nakata, M.D., Department of Radiology, Osaka Medical College, 2–7, Daigaku-cho, Takatsuki, Osaka 569, JAPAN.

MATERIALS AND METHODS

Forty subjects underwent simultaneous anterior and posterior image acquisition, including 6 normal individuals, 16 patients with primary lung cancer, 6 with chronic obstructive pulmonary disease (COPD), 5 with pulmonary embolism, 4 with pneumonia, 2 with tuberculosis and 1 with bronchiectasis. There were 24 males and 16 females with an average age of 59.8 years (range; 13–84 years). The 15 subjects undergoing SPECT included 6 patients with lung cancer, 2 with COPD, 2 with pneumonia and 1 patient each with pulmonary embolism, tuberculosis, angina pectoris, atrial septal defect (ASD), and Fallot's tetralogy. There were 8 males and 7 females with an average age of 47.7 years (range; 14–72 years).

For examination, each patient was placed in the supine position with the arms raised above the head and continuous inhalation of 185 MBq of ^{81m}Kr gas was started. Then 185 MBq of ^{99m}Tc-MAA was administered intravenously. Imaging was performed with a dual-head digital gamma

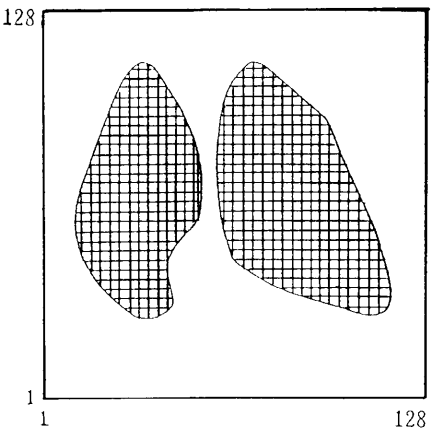

Fig. 1 The 128 × 128 matrix.

$$\%\dot{V}_{Li} = \frac{\dot{V}_{Li}}{\text{SUM } \dot{V}} \times 100 \qquad \text{SUM } \dot{V}\text{: } \dot{V} \text{ in a whole lung}$$

$$\%\dot{V}_{Ri} = \frac{\dot{V}_{Ri}}{\text{SUM } \dot{V}} \times 100 \qquad \text{SUM } \dot{Q}\text{: } \dot{Q} \text{ in a whole lung}$$

$$\%\dot{Q}_{Li} = \frac{\dot{Q}_{Li}}{\text{SUM } \dot{Q}} \times 100 \qquad \text{K: coefficient of correction}$$

$$\%\dot{Q}_{Ri} = \frac{\dot{Q}_{Ri}}{\text{SUM } \dot{Q}} \times 100$$

$$\dot{V}/\dot{Q}_{Li} = \frac{\dot{V}_{Li}}{\dot{Q}_{Li}} \times K \times \frac{\text{SUM } \dot{Q}}{\text{SUM } \dot{V}}$$

$$\dot{V}/\dot{Q}_{Ri} = \frac{\dot{V}_{Ri}}{\dot{Q}_{Ri}} \times K \times \frac{\text{SUM } \dot{Q}}{\text{SUM } \dot{V}}$$

Fig. 2 The formula used for calculation of %$\dot{V}$, %$\dot{Q}$, and the $\dot{V}/\dot{Q}$ ratio.

camera (Toshiba GCA-901A/$_{WB}$) that was equipped with medium-energy high-resolution collimaters permitting simultaneous acquisition of anterior and posterior images. Data processing was performed with a nuclear medicine image processor (Toshiba GMS-550U). SPECT images were acquired with a triple-detector type gamma camera (Toshiba GCA-9300A/$_{HG}$) by rotating the detectors through 360° in 4° steps with the patient in the supine position. As a result, data were acquired in 90 views for 30 sec each. Transverse sections with a thickness of one pixel (3.2 mm) were obtained by the filtered back projection technique. Butterworth and Ramp filters were used to provide adequate noise suppression. Data processing was performed with another nuclear medicine image processor (GMS-5500A). After the region of interest was set to include the entire lungs, the ventilation-perfusion ratio ($\dot{V}/\dot{Q}$ ratio) for each pixel in the region was calculated with a 128 × 128 matrix. A zero count was applied outside the region of interest in the lungs. Using 20% of each maximum count for $\dot{V}$ and $\dot{Q}$ in both lungs as the background value, substraction was performed for each pixel (Fig. 1). The %$\dot{V}$ and %$\dot{Q}$ values were obtained with the formula given below, and the $\dot{V}/\dot{Q}$ ratio was calculated. The correction coefficient for the supine position was assumed to be 1.0 (Fig. 2). The relationships between the $\dot{V}/\dot{Q}$ ratio and %$\dot{V}$, %$\dot{Q}$, or the $\dot{V}/\dot{Q}$ count were displayed in a histogram, and the $\dot{V}/\dot{Q}$ ratio frequency distribution was determined quantitatively. We also superimposed anterior and posterior images, as well as each of the SPECT images.

RESULTS

The $\dot{V}/\dot{Q}$ ratio distribution patterns were classified into the following four types: Type I (the normal distribution, $0.67 \leq \dot{V}/\dot{Q} \leq 1.50$), Type II (a high $\dot{V}/\dot{Q}$ area, $\dot{V}/\dot{Q} > 1.50$ i.e., a dead-space effect), Type III (a low $\dot{V}/\dot{Q}$ area, $\dot{V}/\dot{Q} < 0.67$ i.e., a shunt effect) and Type IV (a mixed pattern). These patterns showed some variation depending on the type of pulmonary disease.

A normal histogram is shown in Figure 3. It has a narrow, symmetrical frequency distribution with a peak $\dot{V}/\dot{Q}$ ratio of 1 when the $\dot{V}/\dot{Q}$ distribution is represented semilogarithmically. In this histogram, $\dot{V}/\dot{Q}$ ratio values are shown within the range divided into 32 sections from 0.25 to 4.0, and results are lumped together for the range less than 0.25 or above 4.0. The abscissa is a logarithmic scale and the ordinate shows the sum of the %$\dot{V}$ value, the %$\dot{Q}$ value, and the $\dot{V}/\dot{Q}$ count corresponding to a particular $\dot{V}/\dot{Q}$ ratio. The $\dot{V}/\dot{Q}$ count data are summed at the maximum value on each graph.

Case 1

An 88-year-old woman with primary lung cancer arising from the left S^6 segment had almost complete obstruction of the left lower bronchus. $\dot{V}/\dot{Q}$ ratio images revealed mismatch caused by this obstruction (Fig. 4 A–G).

Case 2

A 32-year-old man with pulmonary embolism underwent both SPECT and bidirectional imaging. The superimposed coronal SPECT image was compared with the superimposed anterior and posterior images. They showed almost the same findings (Fig. 5 A–F).

As shown in Table 1, the proportion of counts at $\dot{V}/\dot{Q} < 0.67$ (2/3) and/or $\dot{V}/\dot{Q} > 1.50$ (3/2) in the $\dot{V}/\dot{Q}$ counts histogram was compared with overall pulmonary function and blood gas analysis. A significant positive correlation was found between the distribution of the $\dot{V}/\dot{Q}$ ratio histogram and A-aDO_2 for anterior images ($r = 0.684$, $p < 0.05$), posterior images ($r = 0.654$, $p < 0.05$) and superimposed images ($r = 0.696$, $p < 0.05$) (Fig. 6 A–C). In the patients with an increase in A-aDO_2 to >20 Torr ($n = 19$), the correlation was even stronger ($r = 0.715$ for

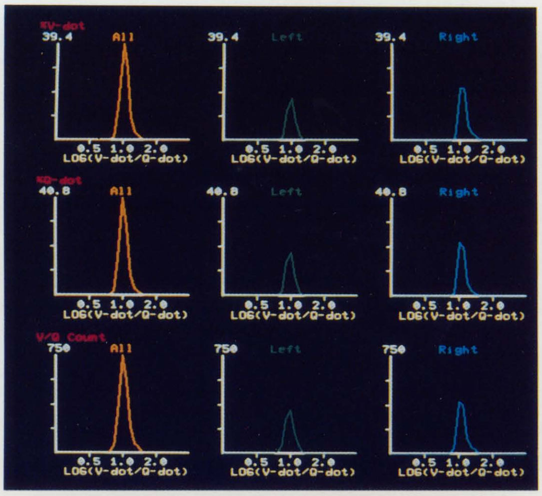

Fig. 3 A normal histogram.

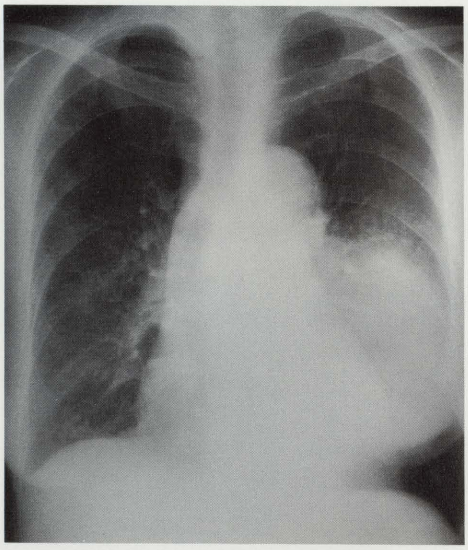

Fig. 4-A Chest X-ray reveals a mass situated in the left lower lung field.

anterior images, r = 0.704 for posterior images, and r = 0.743 for superimposed images: all $p < 0.001$). Superimposed images therefore showed the highest correlation. On the other hand, there was no correlation between lung function and A-aDO_2. In Table 2, superimposed coronal SPECT images and superimposed anterior and posterior images are compared. They showed a good correlation (r = 0.888, $p < 0.001$) with respect to the marked uneven distribution of $\dot{V}/\dot{Q}$ (Fig. 7). In some cases, the SPECT images of the whole lung area could not be obtained and a clear correlation was not observed with A-aDO_2.

DISCUSSION

Alveolar gas exchange is influenced by the ratio of alveolar ventilation volume to pulmonary capillary perfusion volume.[4] In order to evaluate uneven distribution of the ventilation-perfusion ratio, A-aDO_2 is generally measured. $\dot{V}/\dot{Q}$ mismatch is associated with an increase in A-aDO_2. Blood gas analysis (A-aDO_2) gives an indication of the function of both lungs together. In the present study, a correlation between the distribution of the $\dot{V}/\dot{Q}$ histogram and A-aDO_2 was suggested, especially that obtained from superimposed images.

Since the planar image only reflects the function of a relatively superficial portion of the lung, it may be that histograms of superimposed images better reflect the function of the whole lung and A-aDO_2. In fact, a strong positive correlation (r = 0.888, $p < 0.001$) was shown between superimposed anterior and posterior images and superimposed coronal SPECT images in 15 patients. SPECT not only assesses the function of the superficial lung tissue, but also the state of ventilation and perfusion in the deep tissue, and thus can depict defects more clearly than planar images,[5–8] but it requires far more acquisition

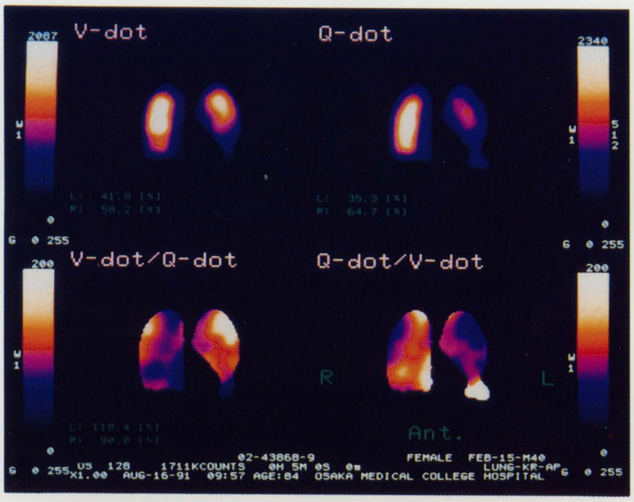

Fig. 4-B The anterior image shows a high $\dot{V}/\dot{Q}$ area in the upper left lung field and a low $\dot{V}/\dot{Q}$ area in the lower lung field.

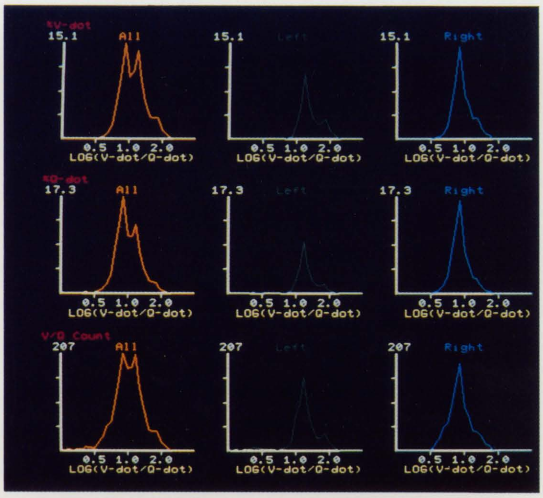

Fig. 4-C The histogram of the anterior image shows a dead-space effect and a mild shunt effect in the left lung.

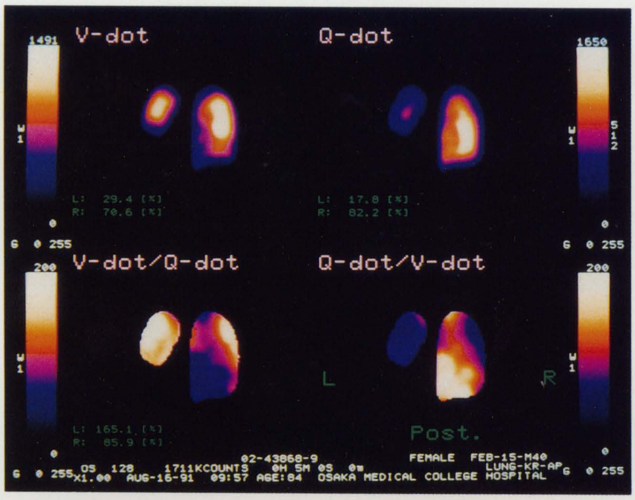

Fig. 4-D The posterior image shows a high $\dot{V}/\dot{Q}$ area in the upper left lung field.

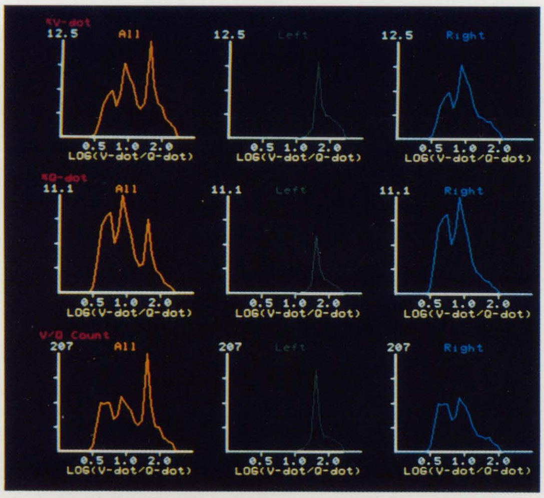

Fig. 4-E The histogram of the posterior image for the left lung shows a dead-space effect and its $\dot{V}/\dot{Q}$ count peak is shifted to the right much more than in the anterior image.

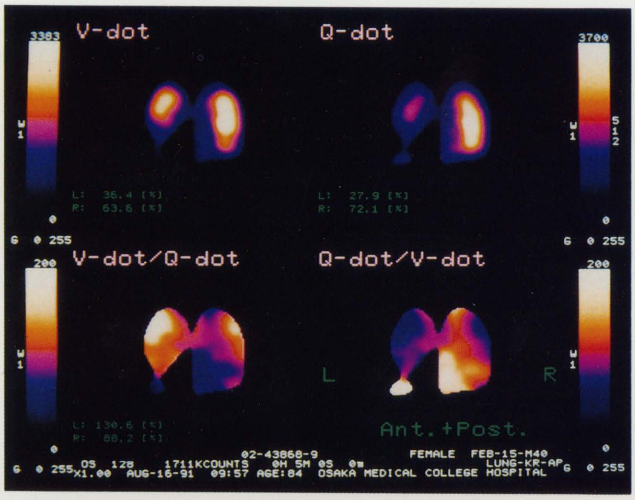

Fig. 4-F A posterior view of superimposed anterior and posterior planar images.

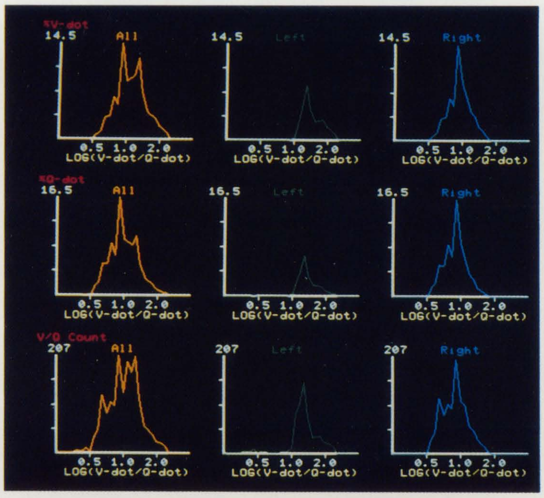

Fig. 4-G The histogram of superimposed anterior and posterior images shows a narrower distribution throughout the entire lung than the posterior image histogram.

time than planar imaging, and analysis of the data is also complicated. Simultaneous anterior and posterior planar image acquisition is simple and noninvasive. Since it achieved a good correlation with SPECT data, this technique seems to be acceptable for pulmonary scintigraphy. Examination of the individual $\dot{V}/\dot{Q}$ histograms for the left and right lungs in various diseases showed that lung cancer mainly caused a Type I or II pattern. In Type I, ventilation was affected as well as perfusion in the area damaged by the tumor. As a result, there was little $\dot{V}/\dot{Q}$ mismatch and the patterns had few or no symptoms. In Type II, a dead-space effect was noted, which agrees with the finding that perfusion is generally more severely affected than ventilation with the progression of the tumor stage.[9–11] Since lung cancer is a localized disease, general pulmonary function tests or blood gas analysis may not reveal any abnormalities. In the case of pulmonary embolism, the entire lung showed a Type IV pattern associated with an increase in A-aDO_2. The decrease in blood flow in the embolized lung tissue resulted in a significant increase in the distribution at $\dot{V}/\dot{Q}$ values below 1.0 in the remaining normal lung tissue and a relative increase in perfusion, i.e., blood flow increased in the nonembolized part of the lung due to a bypass effect.[12,13] Regarding the cause of hypoxemia in pulmonary embolism, a change in perfusion in the nonembolized region is thought to be important.[14] In COPD, a local dead-space effect and a shunt effect were observed,[15] but there was a small but significant shift in $\dot{V}/\dot{Q}$, and a bisferious distribution with a peak around 1.0 was often noted. The increase in A-aDO_2 was therefore thought

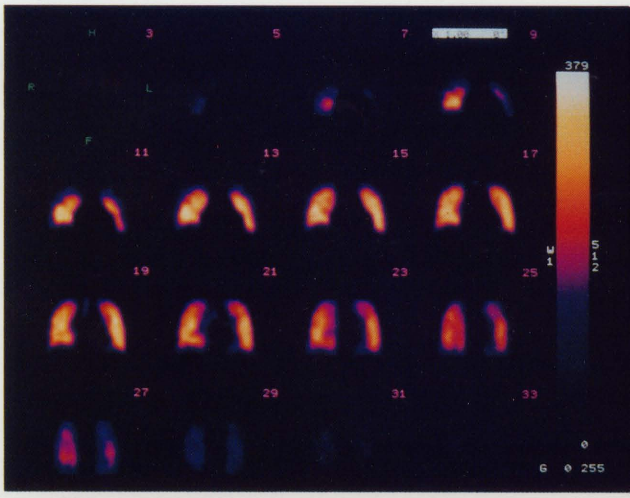

Fig. 5-A A coronal SPECT ventilation image shows almost normal findings.

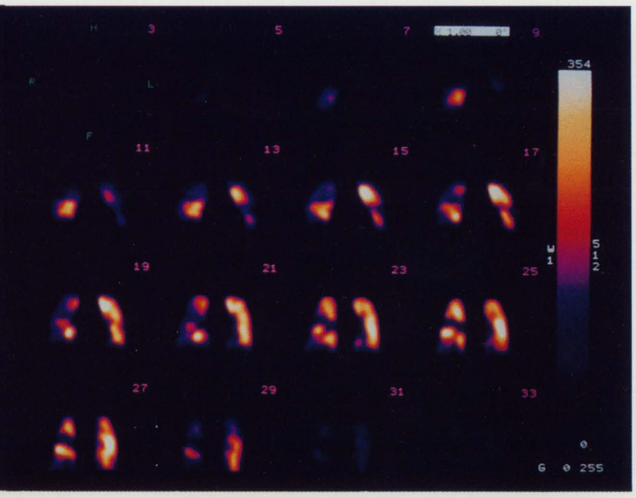

Fig. 5-B A SPECT perfusion image show decreased perfusion in the right middle and lateral lower lung fields and in the left lower lung field.

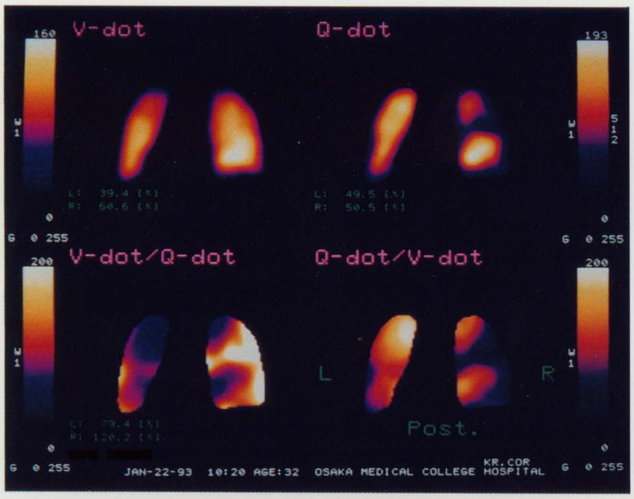

Fig. 5-C A posterior coronal SPECT superimposed image shows a high $\dot{V}/\dot{Q}$ area matched with the perfusion defect.

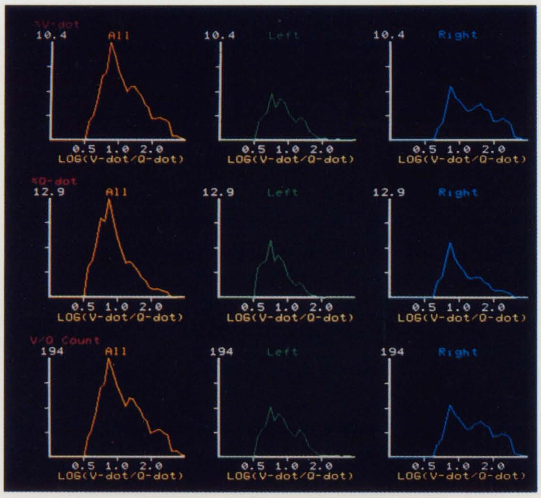

Fig. 5-D A histogram of the SPECT images shows mainly a dead-space effect in the right lung and a shunt effect in the left lung.

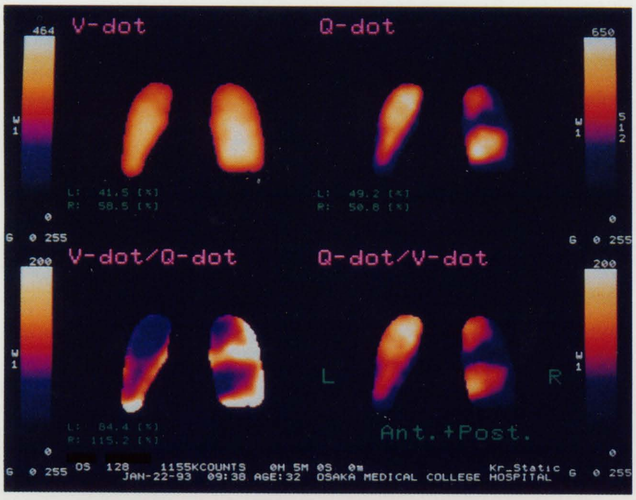

Fig. 5-E A posterior view of superimposed anterior and posterior planar images shows almost the same findings.

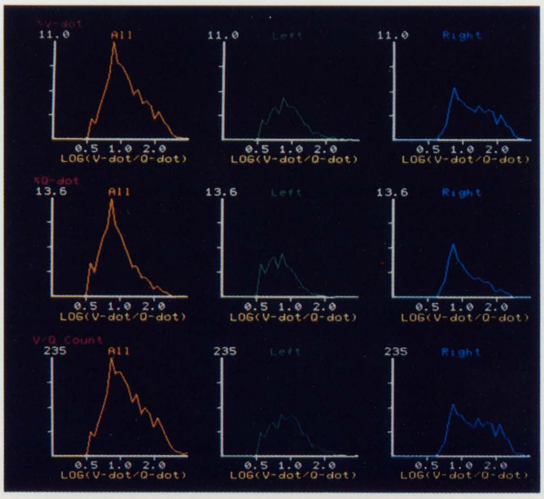

Fig. 5-F A histogram of superimposed anterior and posterior planar images shows almost the same findings.

Table 1 Clinical profile of the 40 subjects undergoing bidirectional planar imaging

case	age	sex	disease	%VC	$FEV_{1.0}$%	A	P	A + P	$A\text{-}aDO_2$
1	74	M	lung cancer	47.0	71.9	5.2	1.6	2.6	11.3
2	84	F	lung cancer	90.7	82.1	24.0	43.7	28.5	32.3
3	80	F	lung cancer	89.7	81.6	0.0	4.2	0.2	1.2
4	62	M	lung cancer			19.6	11.4	10.2	24.3
5	13	M	lung cancer	75.8	84.4	4.8	16.3	7.9	4.6
6	50	M	lung cancer	105.3	73.1	5.6	3.3	5.2	11.5
7	76	F	lung cancer	99.4	62.7	1.4	7.8	2.5	20.8
8	63	M	lung cancer	99.8	27.6	12.9	12.1	11.4	25.4
9	76	M	lung cancer	89.9	67.6	15.5	16.5	13.2	27.1
10	81	M	lung cancer	88.3	64.2	19.4	12.5	17.3	25.8
11	70	F	lung cancer	46.7	81.7	0.4	4.6	0.6	12.6
12	72	M	lung cancer	68.6	42.9	0.0	6.8	1.5	17.2
13	63	M	lung cancer	70.8	87.5	2.9	4.0	2.4	17.9
14	77	M	lung cancer	67.1	94.7	16.4	10.1	8.4	2.6
15	40	M	lung cancer	97.7	82.0	13.4	2.3	7.4	23.5
16	63	M	lung cancer	124.9	84.7	2.9	3.0	2.1	8.7
17	76	F	COPD			24.2	24.4	26.4	34.3
18	59	M	COPD	69.7	30.2	12.8	14.5	10.8	15.8
19	75	F	COPD	55.7	33.2	15.6	9.3	12.2	24.6
20	61	M	COPD	64.0	64.5	11.3	5.2	5.0	13.9
21	78	F	COPD			13.3	15.9	24.5	27.8
22	33	F	COPD	120.4	85.1	0.8	0.7	0.8	10.2
23	49	F	pulmonary embolism	66.5	89.7	37.3	56.3	43.1	28.1
24	56	M	pulmonary embolism	101.2	68.4	79.5	76.0	78.7	35.3
25	43	F	pulmonary embolism	108.9	82.6	46.9	56.7	50.4	26.4
26	31	M	pulmonary embolism			80.0	82.2	80.3	32.6
27	58	F	pulmonary embolism	111.2	79.4	36.2	32.1	32.9	23.6
28	60	M	pneumonia	66.3	87.6	3.6	0.9	3.7	12.9
29	77	M	pneumonia	37.5	92.4	4.8	5.1	2.9	21.4
30	80	M	pneumonia	46.3	92.9	36.7	23.8	28.4	30.4
31	63	F	pneumonia	110.3	67.7	3.4	11.5	5.4	20.7
32	60	F	tuberculosis	85.7	87.0	1.0	0.4	0.2	6.2
33	40	M	tuberculosis	97.7	82.0	13.4	2.3	7.4	23.5
34	69	F	bronchiectasis	93.4	82.8	12.2	7.2	4.5	14.1
35	56	F	none	99.6	82.4	7.5	3.5	7.2	17.0
36	71	F	none			9.0	5.2	3.5	18.6
37	55	M	none	93.6	91.2	0.0	0.0	0.0	8.4
38	64	M	none			4.6	2.8	3.1	6.9
39	63	M	none	91.5	76.2	3.3	2.3	1.1	11.0
40	52	M	none	111.3	75.9	1.6	1.0	0.7	13.7

A: anterior image; P: posterior image
A + P: superimposed anterior and posterior image
$A\text{-}aDO_2$: alveolar-arterial oxygen difference

to be mild. In Fallot's tetralogy (after a Blalock-Taussig operation), the kidney was depicted in perfusion scintigraphy, a right-to-left shunt was proved, and an increase in blood flow through the left pulmonary artery was observed. The left lung histogram indicated displacement of $\dot{V}/\dot{Q}$ below 1.0, and a shunt effect was shown. This phenomenon was thought to be attributable to the Blalock-Taussig procedure, which involves subclavian to left pulmonary artery anastomosis. In general, if there is a right-to-left shunt >15%, the kidney is supposed to be depicted by scintigraphy. Whole body scintigraphy may enable quantitative evaluation of right-to-left shunting in such patients, while preoperative and postoperative examinations may contribute towards assessing the effect of treatment and the state of ventilation and perfusion in each lung. Even if the ventilation and perfusion volumes are equal for the lung as a whole, localized imbalances may lead to the impairment of respiratory function. In view of the results of this study, it seems that more precise information regarding $\dot{V}/\dot{Q}$ mismatch can be obtained both visually and quantitatively in both diffuse and localized lung disease by evaluating separate functional images and histograms for the right and left lungs.

Table 2 Clinical profile of the 15 patients undergoing SPECT

case	age	sex	disease	%VC	$FEV_{1.0}$%	A + P	CORONAL	A-aDO_2
1	38	M	lung cancer	122.2	79.8	2.8	3.5	12.2
2	59	M	lung cancer	72.1	65.4	20.0	26.7	22.4
3	65	M	lung cancer	90.6	85.1	9.7	5.0	21.7
4	72	F	lung cancer	92.4	78.0	20.5	12.8	12.6
5	64	M	lung cancer	80.2	80.8	9.8	9.6	4.3
6	14	F	lung cancer	80.4	66.9	2.9	3.7	6.3
7	60	F	pneumonia	84.1	83.7	6.4	3.5	23.0
8	20	M	pneumonia	114.2	81.2	8.4	8.6	13.6
9	51	M	COPD	81.3	60.2	1.5	7.4	2.4
10	45	F	COPD	116.9	59.5	9.9	6.8	14.2
11	32	M	pulmonary embolism	112.4	81.6	38.5	39.0	25.8
12	60	M	tuberculosis	34.2	72.9	9.4	6.3	6.2
13	50	F	angina pectoris	84.6	77.8	0.9	3.2	10.4
14	51	F	ASD	73.5	65.0	5.5	14.3	24.0
15	34	F	Fallot's tetralogy	66.5	120.3	29.5	20.5	27.5

A + P: superimposed anterior and posterior image
CORONAL: superimposed coronal SPECT image
A-aDO_2: alveolar-arterial oxygen difference

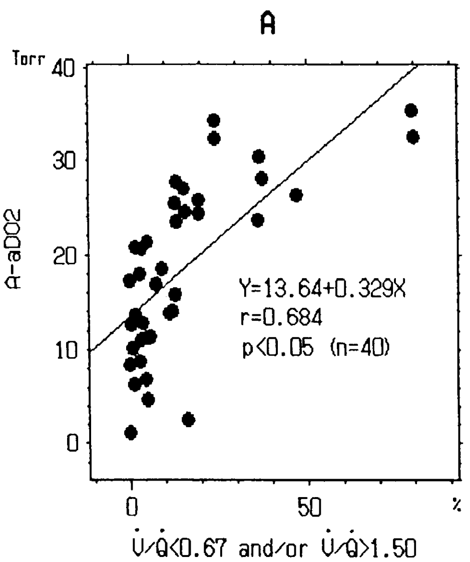

A

Fig. 6 A: The correlation between A-aDO_2 and marked uneven distribution of $\dot{V}/\dot{Q}$ for anterior images.
B: The correlation between A-aDO_2 and marked uneven distribution of $\dot{V}/\dot{Q}$ for posterior images.
C: The correlation between A-aDO_2 and marked uneven distribution of $\dot{V}/\dot{Q}$ for superimposed images.

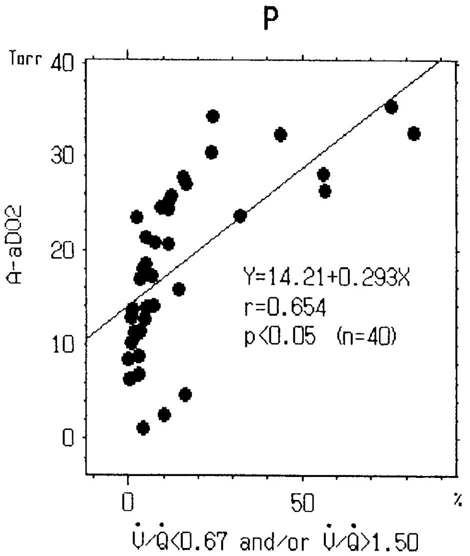

B

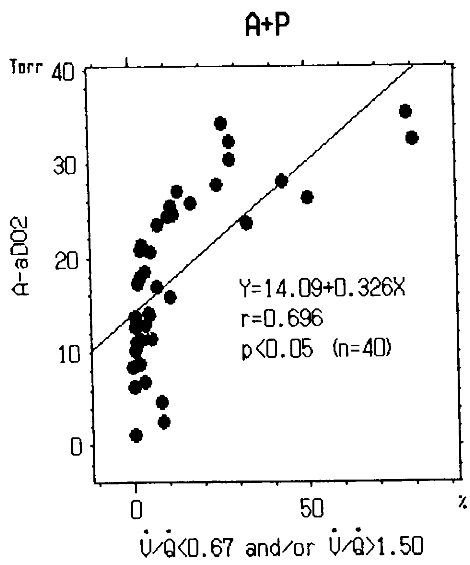

C

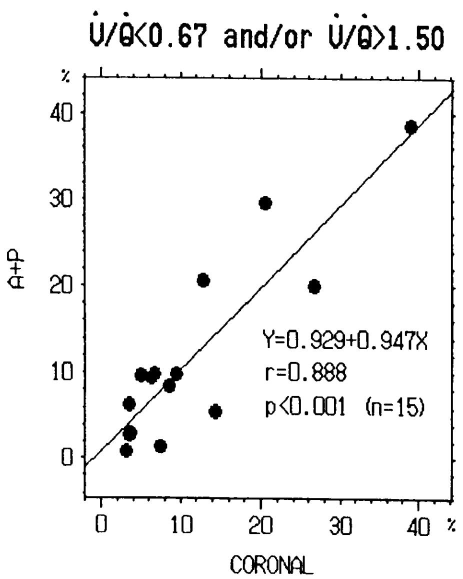

Fig. 7 The correlation of superimposed coronal SPECT images or superimposed anterior and posterior images with marked uneven distribution of $\dot{V}/\dot{Q}$.

CONCLUSION

Simultaneous anterior and posterior image acquisition enabled us to reduce the examining time and showed a good correlation with superimposed coronal SPECT images. We conclude that this technique is simple, noninvasive, and acceptable for the quantitative evaluation of the ventilation-perfusion ratio in various lung diseases.

REFERENCES

1. Fazio F, Pratt TA, McKenzie CG, Steiner RE. Improvement in regional ventilation and perfusion after radiotherapy for unresectable carcinoma of the bronchus. *Am J Roentgenol* 133: 191–200, 1979.
2. Wernly JA, DeMeester TR, Kirchner PT, Myerowitz PD, Oxford FE, Golomb HM. Clinical value of quantitative ventilation-perfusion lung scans in the surgical management of bronchogenic carcinoma. *J Thorac Cardiovasc Surg* 80: 535–543, 1980.
3. Narabayashi I, Otsuka N. Pulmonary ventilation and perfusion studies in lung cancer. *Clin Nucl Med* 9: 97–102, 1984.
4. Suematsu T, Narabayashi I. Imaging diagnosis of gas exchange in patients with lung cancer: evaluation of regional ventilation and perfusion with functional imaging. *Nippon Acta Radiol* 25: 630–640, 1985.
5. Kramer EL, Sanger JJ. ^{81m}Kr gas and ^{99m}Tc-MAA $\dot{V}/\dot{Q}$ ratio images for detection of $\dot{V}/\dot{Q}$ mismatches. *Eur J Nucl Med* 9: 345–350, 1984.
6. Meignan M, Simonneau G, Oliveira L, Harf A, Cinotti L, Cavellier J-F, et al. Conputation of ventilation-perfusion ratio with Kr-81m in pulmonary embolism. *J Nucl Med* 25: 149–151, 1984.
7. Narabayashi I, Suematsu T, Suematsu C. Assessment of SPECT ventilation-perfusion imaging in patients with lung cancer. *Eur J Nucl Med* 12: 329–332, 1986.
8. Rosen JM, Palestro CJ, Markowitz D, Alderson PO. Significance of single ventilation/perfusion mismatches in Krypton-81m/Technetium-99m lung scintigraphy. *J Nucl Med* 27: 361–365, 1986.
9. Svanverg L. Regional functional decrease in bronchial carcinoma. *The Annals of Thoracic Surgery* 3: 170–180, 1972.
10. Secker-Walker RH, Alderson PO, Wilhelm J, Hill RL, Markham J, Kinzie J. Ventilation-perfusion scanning in carcinoma of the bronchus. *Chest* 65: 660–663, 1974.
11. Liscomb DJ, Pride NB. Ventilation and perfusion scans in the preoperative assessment of bronchial carcinoma. *Thorax* 32: 720–725, 1977.
12. Huet Y, Lemaire F, Brun-Buisson C, Knaus WA, Teisseire B, Payen D. Hypoxemin acute pulmonary embolism. *Chest* 88: 829–836, 1985.
13. Tiu S, Liu D, Kramer EL, Sanger JJ. Focal pulmonary edema, correlation with perfusion lung scan. *Clin Nucl Med* 10: 583–585, 1985.
14. Burton GH, Seed WA, Vernon P. Observation on the mechanism of hypoxemia inacute minor pulmonary embolism. *Bri Med J* 289: 276–279, 1984.
15. Wagner PD, Dantzker DR, Dueck R, Clausen JL, West JB. Ventilation-perfusion inequility in chronic obstructive pulmonary disease. *J Clin Invest* 59: 203–216, 1977.